NANO LETTERS
Letter
Cite This: Nano Lett. 2019, 19, 8658−8663
pubs.acs.org/NanoLett

Cu_3N Nanocubes for Selective Electrochemical Reduction of CO_2 to Ethylene

Zhouyang Yin,[†,#] Chao Yu,[†,#] Zhonglong Zhao,[‡] Xuefeng Guo,[†] Mengqi Shen,[†] Na Li,[§] Michelle Muzzio,[†] Junrui Li,[†] Hu Liu,[†] Honghong Lin,[†] Jie Yin,[†] Gang Lu,[‡] Dong Su,[§] and Shouheng Sun*[,†]

[†]Department of Chemistry, Brown University, Providence, Rhode Island 02912, United States
[‡]Department of Physics and Astronomy, California State University Northridge, Northridge, California 91330, United States
[§]Center for Functional Nanomaterials, Brookhaven National Laboratory, Upton, New York 11973, United States

Supporting Information

ABSTRACT: Understanding the Cu-catalyzed electrochemical CO_2 reduction reaction (CO_2RR) under ambient conditions is both fundamentally interesting and technologically important for selective CO_2RR to hydrocarbons. Current Cu catalysts studied for the CO_2RR can show high activity but tend to yield a mixture of different hydrocarbons, posing a serious challenge on using any of these catalysts for selective CO_2RR. Here, we report a new perovskite-type copper(I) nitride (Cu_3N) nanocube (NC) catalyst for selective CO_2RR. The 25 nm Cu_3N NCs show high CO_2RR selectivity and stability to ethylene (C_2H_4) at −1.6 V (vs reversible hydrogen electrode (RHE)) with the Faradaic efficiency of 60%, mass activity of 34 A/g, and C_2H_4/CH_4 molar ratio of >2000. More detailed electrochemical characterization, X-ray photon spectroscopy, and density functional theory calculations suggest that the high CO_2RR selectivity is likely a result of (100) Cu(I) stabilization by the Cu_3N structure, which favors CO−CHO coupling on the (100) Cu_3N surface, leading to selective formation of C_2H_4. Our study presents a good example of utilizing metal nitrides as highly efficient nanocatalysts for selective CO_2RR to hydrocarbons that will be important for sustainable chemistry/energy applications.

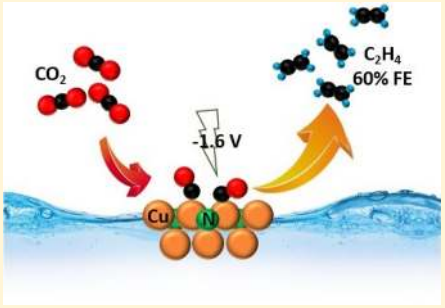

KEYWORDS: *CO_2 reduction, copper(I) nitride, perovskite structure, nanocubes, ethylene formation*

Active and selective CO_2 reduction reaction (CO_2RR) is an essential step to recycle the overproduced CO_2 back to reusable forms of carbon and to build an energy-sustainable society.[1−3] Electrochemical CO_2RR can proceed under ambient conditions and has been studied extensively to understand catalysis fundamentals and to develop efficient catalysts for practical applications.[4−8] Among all nanostructured catalysts tested thus far, nanostructured Cu catalysts are unique to catalyze CO_2RR to hydrocarbons.[9−14] However, past studies also show that it is difficult to control Cu surface catalysis under ambient conditions, and the reaction often leads to the formation of a mixture of hydrocarbons, which makes the separation of a specific hydrocarbon product extremely challenging. Recently, a flow-cell design was used to convert CO_2 more selectively to hydrocarbons, especially to ethylene (C_2H_4) with the Faradaic efficiency (FE) reaching up to 70%.[15,16] However, this cell device does require corrosive alkaline electrolyte, such as 10 M KOH, to realize the desired conversion.

Here, we introduce perovskite-structured copper(I) nitride (Cu_3N) nanocubes (NCs) as a new catalyst for selective CO_2RR to ethylene (C_2H_4) under ambient conditions. Nanostructured transition metal nitrides have been studied for electrocatalytic reactions,[17,18] but a very limited number of metal nitrides were tested for CO_2RR. Ni_3N was studied for CO_2RR to CO.[19] Cu_3N nanowires prepared from nitridation of $Cu(OH)_2$ nanowires were converted to multigrained Cu nanowires to show high CO_2RR selectivity to C_2 products[20] due likely to the semiconductivity of Cu_3N.[21] Different from these nitride catalysts, our Cu_3N NCs have a phase-pure anti-ReO_3 perovskite-type structure,[22] and in 0.1 M $KHCO_3$ electrolyte solution, they catalyze the CO_2RR to C_2H_4 with 60% FE and 34 A/g Cu mass activity at −1.6 V vs RHE. More importantly, the NC catalyst suppresses the formation of CH_4 in the gas-phase products with a C_2H_4/CH_4 molar ratio of >2000, the highest selectivity ever reported for Cu-based CO_2RR catalysis. Our Cu_3N NC structure is also stable in the CO_2RR condition, showing only 7% FE decrease (from 60 to 53%) under continuous electrolysis for 20 h. The combined ease of synthesis and high CO_2RR catalytic selectivity and durability make the Cu_3N NCs a promising new catalyst for practical CO_2RR to C_2H_4, an important industry feedstock used to produce ethylene oxide, ethylene dichloride, ethylbenzene, and polyethylene.

Received: August 13, 2019
Revised: September 26, 2019
Published: November 4, 2019

DOI: 10.1021/acs.nanolett.9b03324
Nano Lett. 2019, 19, 8658−8663

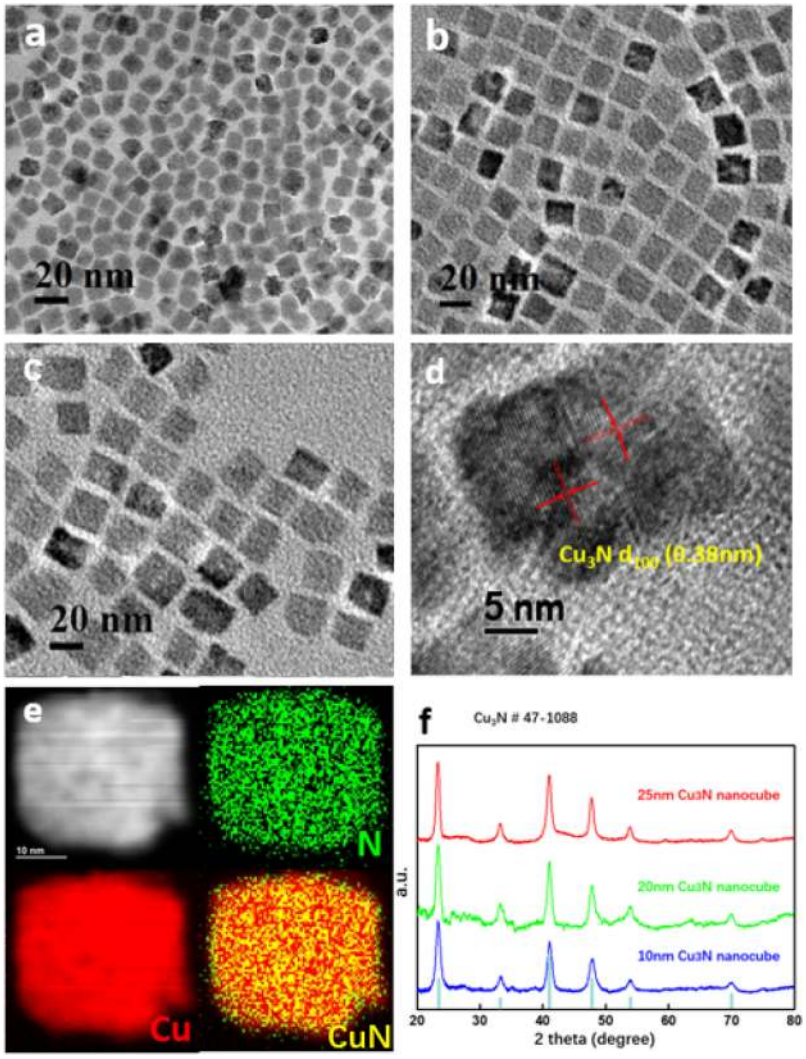

Figure 1. Characterizations of Cu_3N NCs. (a–c) Low-resolution TEM images of the as-synthesized 10 nm (a), 20 nm (b), and 25 nm (c) Cu_3N NCs. (d) High-resolution TEM image of a representative 25 nm Cu_3N NC, showing lattice fringe along the ⟨100⟩ direction. (e) HAADF-STEM image of Cu_3N NC and the corresponding STEM-EELS elemental mapping of the NC. (f) XRD patterns of the 10, 20, and 25 nm Cu_3N NCs, showing typical diffraction patterns that correspond to the perovskite-type *Pm*3*m* structure.

Cu_3N NCs were synthesized by modifying a published method.[23] First, 25 nm Cu_3N NCs were prepared by partially reducing $Cu(NO_3)_2{\cdot}3H_2O$ with octadecylamine/oleylamine (2.5*g*/2.5 mL, ∼1/0.8 mass ratio; see Supporting Information for details) at 240 °C, whereas 20 and 10 nm NCs were made at 250 and 260 °C, respectively. These synthetic results indicate that higher reaction temperature initiates faster nucleation, consuming more Cu precursor in the nucleation stage and leading to the formation of smaller NCs. Another observation is that the formation of cubic Cu_3N requires the reaction temperature to be at 240 °C or above. Low reaction temperatures took longer times for the Cu precursor to nucleate, and the Cu_3N seeds obtained from this slow nucleation event may be defected. It is difficult for the defected seeds to grow into NCs.[24] As a result, at 230 °C, 20 nm sphere-like Cu_3N nanoparticles (NPs) were separated. Figure 1a–c shows transmission electron microscopy (TEM) images of the as-synthesized Cu_3N NCs with lateral dimensions at 9.7 ± 0.4, 20.0 ± 0.7, and 25.0 ± 1.5 nm, and Figure S1 shows the TEM image of the 20 nm Cu_3N NPs. High-resolution TEM (HRTEM) of a representative 25 nm Cu_3N NC (Figure 1d) shows clear lattice fringes with their interfringe distance at 0.38 nm, which is close to interplanar distance of the (100) planes of the cubic Cu_3N *Pm*3*m* structure. High-angle annular dark-field scanning TEM (HAADF-STEM) and STEM electron energy loss spectroscopy (STEM-EELS) (Figure 1e) show that the Cu and N are uniformly distributed across the cubic structure. X-ray diffraction (XRD) patterns of the 10, 20, and 25 nm Cu_3N NC powders further confirms that the NCs have the cubic *Pm*3*m* structure (Figure 1f), which is an anti-ReO_3 perovskite structure.[22] These Cu_3N NCs are colloidally and chemically stable under ambient conditions as they showed neither aggregation nor obvious sign of surface oxidation 2 weeks after their hexane dispersion was exposed to air (Figure S2). Annealed at 200 °C under Ar for 2 h, the Cu_3N NCs showed no structure change (Figure S3), but at 300 °C for 2 h, they were converted to Cu NPs (Figure S4), which was further confirmed by thermal gravimetric analysis (TGA) (Figure S5). As these Cu_3N NCs are stable under ambient conditions, they are a viable catalyst for studying CO_2RR.

DOI: 10.1021/acs.nanolett.9b03324
Nano Lett. 2019, 19, 8658–8663

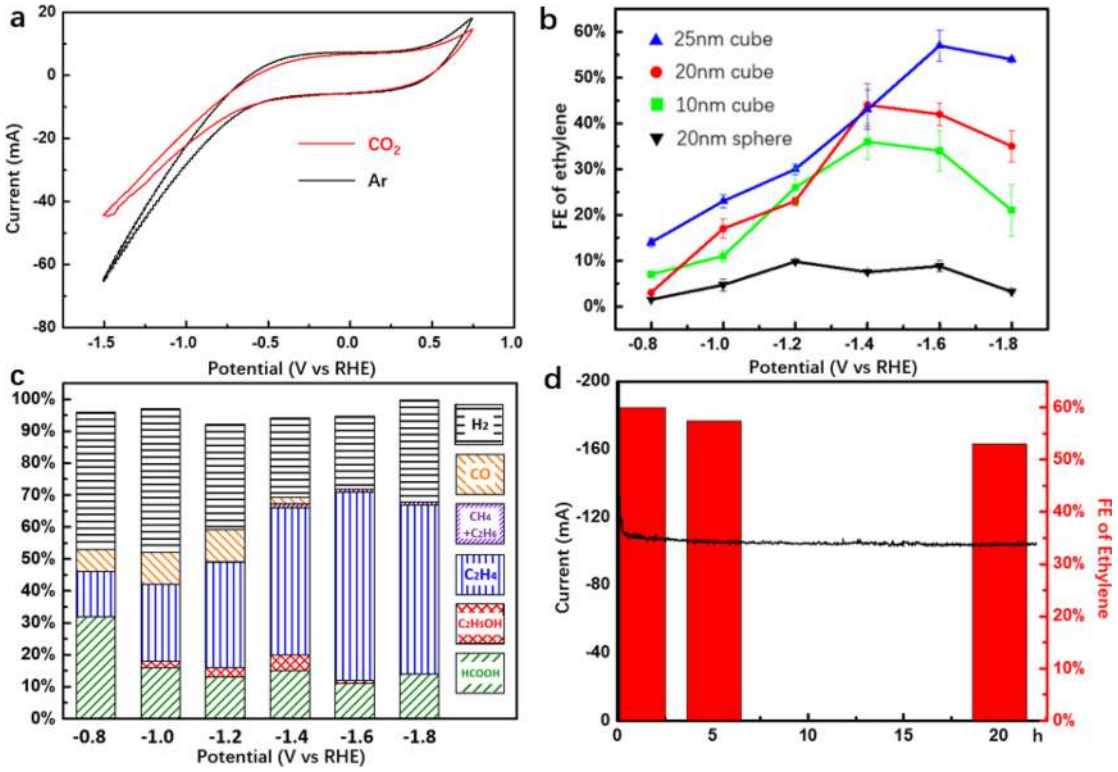

Figure 2. Cu_3N-catalyzed CO_2RR in 0.1 M $KHCO_3$ solution. (a) CV curves of Cu_3N NCs under Ar (black) and CO_2 (red) atmosphere. (b) Potential-dependent ethylene formation FE of CO_2RR catalyzed by different Cu_3N catalysts. (c) Products distribution of CO_2RR catalyzed by 25 nm Cu_3N NC catalyst at different reduction potentials. (d) Reduction current change (black) and ethylene formation FE (red) over time during the continuous CO_2RR catalyzed by 25 nm NCs at −1.6 V.

The Cu_3N NCs were deposited on Ketjen carbon (Figure S6) and painted on carbon paper (Toray TGP-H-060) for electrochemistry and electrocatalytic CO_2RR studies in 0.1 M $KHCO_3$ (see Supporting Information for details). The cyclic voltammetry (CV) curve of the 25 nm Cu_3N NCs under an Ar atmosphere shows no Cu redox peaks (Figure 2a), which is different from what is commonly observed from the Cu NP catalyst,[25] indicating that there is no measurable metallic Cu on the Cu_3N NC surface. Other Cu_3N NCs and Cu_3N NPs show similar CV behaviors (Figure S7). The increased current after −0.5 V is attributed to proton reduction (hydrogen evolution reaction (HER)). CV under CO_2 atmosphere is similar to that under Ar condition except the decrease of the current after −0.5 V (Figure 2a) due to the competition between CO_2RR and HER.[26]

With continuous CO_2 flow, electrochemical CO_2RR was tested under different potentials, and the gas/liquid products were characterized by gas chromatography and ^1H NMR (see Supporting Information for details). The potential-dependent FEs of C_2H_4 formed in the presence of different Cu_3N catalysts are listed in Figure 2b. The general trend is that the larger the NCs, the better the CO_2RR selectivity. Other smaller NCs are less effective, and their peak FEs reach 45% (20 nm NCs) and 35% (10 nm NCs) at −1.4 V. The spherical 20 nm Cu_3N NP catalyst is least active with the FE of C_2H_4 being less than 10% in the reduction potential range tested. The 25 nm Cu_3N-catalyzed CO_2RR generates C_2H_4 (14% FE) at −0.8 V. At −1.6 V, the FE of C_2H_4 reaches the maximum 60% with the mass activity of 34 A/g and current density of 30 mA/cm^2 (Figure S8), and their overall CO_2RR results are summarized in Figure 2c. In addition to C_2H_4, the gas products obtained from various reduction potentials also contain H_2 (<40% FE) from HER and CO (<9% FE) (CO was undetectable at −1.6 V or beyond). The liquid-phase products separated from the reaction contain only formate (<33% FE) and ethanol (<5.7% FE) over the potential range we studied. The 25 nm Cu_3N-catalyzed CO_2RR is most selective at −1.6 V for generating C_2H_4 (60%) with remarkable current density (the ^1H NMR spectrum of the corresponding minor liquid products HCOOH and ethanol is shown in Figure S9.). We measured the capacitive behaviors of the Cu_3N NCs in a potential range from −0.05 to 0.05 V at different scanning rates and obtained their double-layer capacitance of 4.34 mF/cm^2 (Figure S10), which is 150 times larger than the standard capacitance of the smooth Cu electrode (0.029 mF),[27] suggesting that high current density observed from the CO_2RR originates from the large electrochemical surface area of the NC electrode.

We should note that, compared with the common Cu metal catalyst, our Cu_3N catalyst shows higher CO_2RR overpotentials due most likely to the decrease in electron conductivity of the Cu_3N structure. However, because 25 nm Cu_3N NCs are more active and selective than smaller Cu_3N NCs or Cu_3N NPs for the CO_2RR to C_2H_4, it is evident that Cu_3N NCs with larger fractions of (100) facets are especially selective to catalyze CO_2RR to C_2H_4. Another important feature of the Cu_3N NC catalysis is that the catalyst suppresses the formation of C_2H_6 and CH_4 (only <1% FE of C_2H_6 + CH_4 was detected) and shows the highest C_2H_4/CH_4 ratio (>2000) ever reported for the Cu-catalyzed CO_2RR.[28]

The stability of the Cu_3N-catalyzed CO_2RR was studied at −1.6 V (Figure 2d). The reduction current decreased from 135 mA in the first hour to 101 mA 20 h after the continued

DOI: 10.1021/acs.nanolett.9b03324
Nano Lett. 2019, 19, 8658−8663

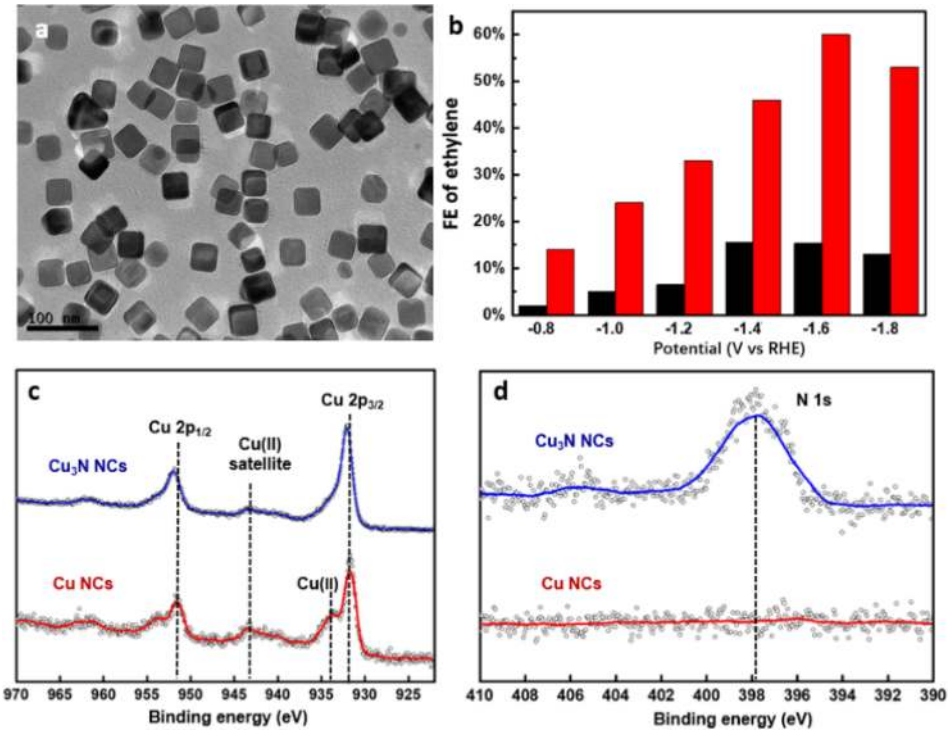

Figure 3. Catalytic performance and surface properties of Cu and Cu_3N catalysts. (a) TEM image of as-synthesized 29 nm Cu NCs. (b) Reduction-potential-dependent FE of ethylene obtained from CO_2RR catalyzed by 25 nm Cu_3N NCs (red) and 29 nm Cu NCs (black). (c) XPS of Cu and Cu_3N NCs showing Cu 2p and Cu(II) peaks. Cu/Cu(I) peaks are too close to separate from the spectra. (d) XPS of Cu and Cu_3N NCs showing N 1s binding energy.

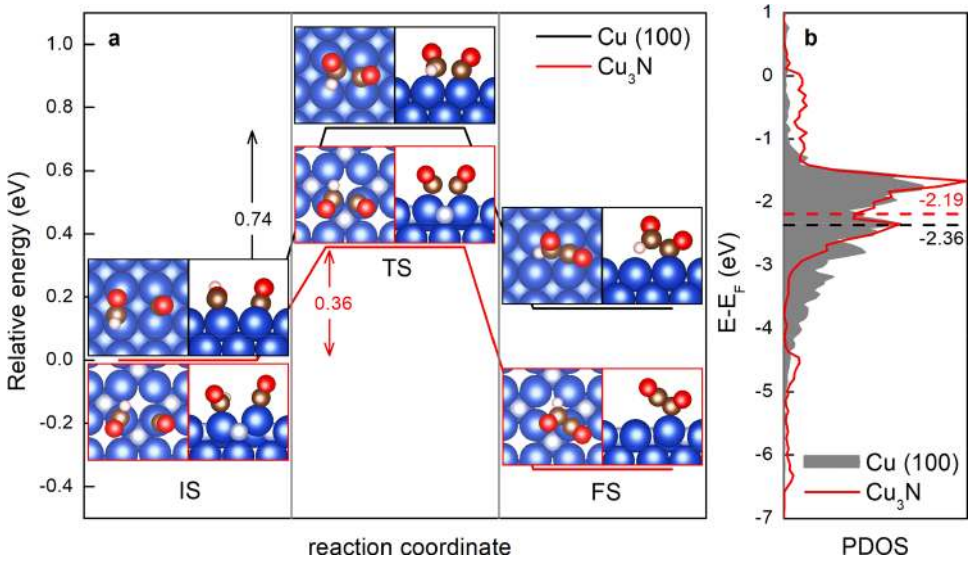

Figure 4. Relative free energy diagram and electronic density of states. (a) Relative free energy diagram for the coupling between CHO_{ads} and CO_{ads} on the Cu(100) and Cu_3N(100) surfaces, respectively. The optimized atomic geometries of the initial, transition, and final states are shown in the insets. Blue, blue gray, gray, red, and white spheres represent Cu, N, C, O, and H atoms, respectively. (b) Calculated density of states of the d-band on the Cu(100) and Cu_3N(100) surfaces. The horizontal dashed lines indicate the d-band centers.

electrolysis. The C_2H_4 formation FE was at 60% in the first hour and was stabilized at around 53%. The TEM image of the Cu_3N NCs after the 20 h of electrolysis (Figure S11) shows that there is only a small degree of NC aggregation, which supports why there is the 7% FE decrease from 60 to 53% during the 20 h electrolysis at −1.6 V. Compared to Cu-based nanocatalysts, especially Cu NCs,[29−31] reported previously with very limited stability in the selected CO_2RR condition, our Cu_3N NCs show much enhanced stability, suggesting that N^{3-} stabilizes Cu^+ more efficiently in the perovskite-type Cu_3N structure.

To confirm that the high CO_2RR selectivity to C_2H_4 is from the Cu_3N(100) and not from Cu(100), we prepared 29.3 ± 3.2 nm Cu NCs, denoted as 29 nm Cu NCs (Figure 3a),[32] and studied/compared their electrochemical CO_2RR with 25 nm Cu_3N NCs. As seen in Figure 3b, on Cu NCs, C_2H_4 is

DOI: 10.1021/acs.nanolett.9b03324
Nano Lett. 2019, 19, 8658−8663

produced starting from −0.8 V, and the highest FE of C_2H_4 is about 15.4% at −1.4 V. As a comparison, the Cu_3N NCs show much higher CO_2RR selectivity to C_2H_4 in all reduction potentials from −0.8 to −1.8 V. As both 29 nm Cu NCs and 25 nm Cu_3N NCs have similar sizes and cube morphology, the superior CO_2RR performance of Cu_3N NCs over Cu NCs suggests that the Cu−N units in the Cu_3N NC structure is essential for the NCs to achieve high CO_2RR selectivity toward C_2H_4.

To identify which Cu oxidation state, Cu(0) or Cu(I), on the Cu_3N surface dominates the CO_2RR selectivity, we studied surface Cu oxidation and reduction properties of both Cu and Cu_3N NCs using X-ray photoelectron spectroscopy (XPS) and CV. The XPS of Cu NCs shows typical Cu 2p peaks at 932 and 952 eV, as well as two Cu(II) peaks at 934 and 944 eV (Figure 3c), but they are free from N 1s peak (Figure 3d), indicating that the Cu NC surface has Cu, Cu(I), and Cu(II) components. Cu_3N NCs also show two Cu 2p peaks that slightly shift to higher energies and a nearly invisible Cu(II) peak. This indicates that, unlike Cu NCs, the Cu_3N NCs have Cu(I) enriched on their surfaces. The N 1s peak is around 398 eV (Figure 3d), close to the common value (∼397 eV) observed from metal nitrides. CV of the Cu NCs in Ar-saturated 0.1 M $KHCO_3$ solution exhibit two reduction peaks at 0.35 V (Cu(II)/(Cu(I)) and −0.05 V (Cu(I)/Cu) (Figure S12), indicating that the Cu NC surface after the oxidation scan is surrounded with Cu(II) and Cu(I). These two reduction peaks shift to more positive potentials under CO_2-saturated conditions due likely to the CO_2 interaction with Cu(I)/Cu(II). Under the same CV scanning condition, Cu_3N NCs show no obvious reduction peaks (Figure 2a), indicating that, on the Cu_3N surface, Cu^+ is better stabilized by N^{3-}, and Cu−N must show the desired synergistic effect on selective CO_2RR to C_2H_4.

We performed density functional theory (DFT) calculations to elucidate why Cu_3N NCs are so selective for the CO_2RR to C_2H_4. As C−C coupling is essential for the formation of C_2 products, such as C_2H_4, we focus on the relevant C−C coupling reactions on the $Cu_3N(100)$ surface. Previous work[33] has established that the C−C bond can be formed on a Cu(100) surface via the coupling between two CO* molecules (to form $OCCO_{ads}$) or between CHO* and CO* (to form $OCCHO_{ads}$). Our calculations show that the CO−CO coupling is not favored on the $Cu_3N(100)$ surface, whereas the CO−CHO coupling has the energy benefits, as shown in Figure 4a. The free energy barrier for the formation of $OCCHO_{ads}$ on the $Cu_3N(100)$ surface is 0.36 eV, less than half of that on the Cu(100) surface (0.74 eV). From the atomic structures of the initial, transition, and final states of the CHO−CO coupling reaction (inset of Figure 4a), we can see that, on the Cu(100) surface, CHO_{ads}, CO_{ads}, and $OCCHO_{ads}$ occupy the Cu bridge sites, whereas on the $Cu_3N(100)$ surface, they are stabilized on the Cu(I) top sites due likely to the upshift of the Cu d-band center on the Cu_3N surface relative to the Cu(100) surface (Figure 4b), as well as the N^{3-}-induced protonation of CO to CHO. The high energy barrier for the CO−CO coupling on the Cu_3N surface suggests that the CO−CO pathway leading to the formation of C_2 products is suppressed, leaving the CO−CHO coupling a dominant pathway to C_2H_4.[34−36]

In this work, we report a new catalyst based on Cu_3N NCs for electrochemical CO_2RR. Among 10, 20, and 25 nm NCs studied, the 25 nm Cu_3N NCs show the highest activity and selectivity to convert CO_2 to C_2H_4 with FE reaching 60%. More importantly, at the C_2H_4 formation potential (−1.6 V), C_2H_4 is the dominant gas product with the C_2H_4/CH_4 ratio being >2000, and liquid products contain mostly formate (<15% FE), which makes the separation of C_2H_4 from the CO_2RR practical. Our studies confirm that Cu(I) is stabilized by N in the Cu_3N structure, and the stabilized Cu(I) is key for the (100) Cu(I) to show enhanced CO_2RR selectivity to C_2H_4. DFT calculations suggest that the stabilized (100) Cu(I) sites are energetically favored for CO−CHO (not CO−CO) coupling, inferring that the formation of $COCHO_{ads}$ is a dominant pathway in the Cu_3N-catalyzed CO_2RR to C_2H_4. This Cu_3N-induced catalysis enhancement on selective CO_2RR may offer a new direction to develop highly efficient nanocatalysts for selective CO_2RR to C_2H_4 or other hydrocarbons.

■ ASSOCIATED CONTENT

Supporting Information

The Supporting Information is available free of charge on the ACS Publications website at DOI: 10.1021/acs.nanolett.9b03324.

Experimental procedures and supporting Figures S1−S12 (PDF)

■ AUTHOR INFORMATION

Corresponding Author

*E-mail: ssun@brown.edu.

ORCID

Chao Yu: 0000-0002-4028-4250
Zhonglong Zhao: 0000-0002-2245-9045
Xuefeng Guo: 0000-0001-5358-4108
Mengqi Shen: 0000-0001-9265-6784
Junrui Li: 0000-0002-4386-1199
Hu Liu: 0000-0002-5237-6419
Dong Su: 0000-0002-1921-6683
Shouheng Sun: 0000-0002-4051-0430

Author Contributions

#Z.Y. and C.Y. contributed equally to this work.

Funding

The work was supported by the American Chemical Society Petroleum Research Fund (57114-ND5) and in part by the Center for the Capture and Conversion of CO_2, a Center for Chemical Innovation funded by the National Science Foundation, CHE-1240020. M.M. is supported by the National Science Foundation Graduate Research Fellowship, under Grant No. 1644760. The electron microscopy work used resources of the Center for Functional Nanomaterials, which is a U.S. DOE Office of Science Facility, at Brookhaven National Laboratory under Contract No. DE-SC0012704. The work at California State University Northridge was supported by the National Science Foundation, DMR-1828019.

Notes

The authors declare no competing financial interest.

■ REFERENCES

(1) Kondratenko, E. V.; Mul, G.; Baltrusaitis, J.; Larrazábal, G. O.; Pérez-Ramírez, J. Status and Perspectives of CO_2 Conversion into Fuels and Chemicals by Catalytic, Photocatalytic and Electrocatalytic Processes. *Energy Environ. Sci.* **2013**, *6*, 3112−3135.

DOI: 10.1021/acs.nanolett.9b03324
Nano Lett. 2019, 19, 8658−8663

(2) Xu, S.; Carter, E. A. Theoretical Insights into Heterogeneous (Photo)electrochemical CO_2 Reduction. *Chem. Rev.* **2019**, *119*, 6631−6669.
(3) Barton, E. E.; Rampulla, D. M.; Bocarsly, A. B. Selective Solar-driven Reduction of CO_2 to Methanol Using a Catalyzed p-GaP based Photoelectrochemical Cell. *J. Am. Chem. Soc.* **2008**, *130*, 6342−6344.
(4) Costentin, C.; Robert, M.; Saveant, J. M. Catalysis of the Electrochemical Reduction of Carbon Dioxide. *Chem. Soc. Rev.* **2013**, *42*, 2423−2436.
(5) Hori, Y.; Kikuchi, K.; Suzuki, S. Production of CO and CH_4 in Electrochemical Reduction of CO_2 at Metal-Electrodes in Aqueous Hydrogencarbonate Solution. *Chem. Lett.* **1985**, *14*, 1695−1698.
(6) Zhu, W.; Michalsky, R.; Metin, O.; Lv, H.; Guo, S.; Wright, C. J.; Sun, X.; Peterson, A. A.; Sun, S. Monodisperse Au Nanoparticles for Selective Electrocatalytic Reduction of CO_2 to CO. *J. Am. Chem. Soc.* **2013**, *135*, 16833−16836.
(7) Zhu, W.; Zhang, Y. J.; Zhang, H.; Lv, H.; Li, Q.; Michalsky, R.; Peterson, A. A.; Sun, S. Active and Selective Conversion of CO_2 to CO on Ultrathin Au Nanowires. *J. Am. Chem. Soc.* **2014**, *136*, 16132−16135.
(8) Wang, L.; Nitopi, S. A.; Bertheussen, E.; Orazov, M.; Morales-Guio, C. G.; Liu, X.; Higgins, D. C.; Chan, K.; Nørskov, J. K.; Hahn, C.; Jaramillo, T. F. Electrochemical Carbon Monoxide Reduction on Polycrystalline Copper: Effects of Potential, Pressure, and pH on Selectivity toward Multicarbon and Oxygenated Products. *ACS Catal.* **2018**, *8*, 7445−7454.
(9) Reske, R.; Mistry, H.; Behafarid, F.; Roldan Cuenya, B.; Strasser, P. Particle Size Effects in the Catalytic Electroreduction of CO_2 on Cu Nanoparticles. *J. Am. Chem. Soc.* **2014**, *136*, 6978−6986.
(10) Zhou, Y.; Che, F.; Liu, M.; Zou, C.; Liang, Z.; De Luna, P.; Yuan, H.; Li, J.; Wang, Z.; Xie, H.; et al. Dopant-induced Electron Localization Drives CO_2 Reduction to C2 Hydrocarbons. *Nat. Chem.* **2018**, *10*, 974−980.
(11) Li, C. W.; Ciston, J.; Kanan, M. W. Electroreduction of Carbon Monoxide to liquid fuel on Oxide-derived Nanocrystalline Copper. *Nature* **2014**, *508*, 504−507.
(12) Liang, Z. Q.; Zhuang, T. T.; Seifitokaldani, A.; Li, J.; Huang, C. W.; Tan, C. S.; Li, Y.; De Luna, P.; Dinh, C. T.; Hu, Y.; et al. Copper-on-nitride Enhances the Stable Electrosynthesis of Multi-Carbon Products from CO_2. *Nat. Commun.* **2018**, *9*, 3828.
(13) Gao, D.; Arán-Ais, R. M.; Jeon, H. S.; Roldan Cuenya, B. Rational Catalyst and Electrolyte Design for CO_2 Electroreduction towards Multicarbon Products. *Nat. Catal.* **2019**, *2*, 198−210.
(14) Lum, Y.; Ager, J. W. Evidence for Product-specific Active Sites on Oxide-derived Cu Catalysts for Electrochemical CO_2 Reduction. *Nat. Catal.* **2019**, *2*, 86−93.
(15) Dinh, C. T.; Burdyny, T.; Kibria, M. G.; Seifitokaldani, A.; Gabardo, C. M.; Garcia de Arquer, F. P.; Kiani, A.; Edwards, J. P.; De Luna, P.; Bushuyev, O. S.; et al. CO_2 Electroreduction to Ethylene via Hydroxide-mediated Copper Catalysis at an Abrupt Interface. *Science* **2018**, *360*, 783−787.
(16) Jouny, M.; Luc, W.; Jiao, F. High-rate Electroreduction of Carbon Monoxide to Multi-Carbon Products. *Nat. Catal.* **2018**, *1*, 748−755.
(17) Wu, H. B.; Chen, W. Copper Nitride Nanocubes: Size-Controlled Synthesis and Application as Cathode Catalyst in Alkaline Fuel Cells. *J. Am. Chem. Soc.* **2011**, *133*, 15236−15239.
(18) Dong, S.; Chen, X.; Zhang, X.; Cui, G. Nanostructured Transition Metal Nitrides for Energy Storage and Fuel Cells. *Coord. Chem. Rev.* **2013**, *257*, 1946−1956.
(19) Hou, P.; Wang, X.; Wang, Z.; Kang, P. Gas Phase Electrolysis of Carbon Dioxide to Carbon Monoxide Using Nickel Nitride as the Carbon Enrichment Catalyst. *ACS Appl. Mater. Interfaces* **2018**, *10*, 38024−38031.
(20) Mi, Y.; Shen, S.; Peng, X.; Bao, H.; Liu, X.; Luo, J. Selective Electroreduction of CO_2 to C2 Products over Cu_3N-Derived Cu Nanowires. *ChemElectroChem* **2019**, *6*, 2393−2397.
(21) Matsuzaki, K.; Harada, K.; Kumagai, Y.; Koshiya, S.; Kimoto, K.; Ueda, S.; Sasase, M.; Maeda, A.; Susaki, T.; Kitano, M.; et al. High-Mobility p-Type and n-Type Copper Nitride Semiconductors by Direct Nitriding Synthesis and In Silico Doping Design. *Adv. Mater.* **2018**, *30*, 1801968.
(22) Juza, R.; Hahn, H. Crystal Structures of Cu_3N, GaN and InN - Metallic Amides and Metallic Nitrides V Announcement. *Z. Anorg. Allg. Chem.* **1938**, *239*, 282−287.
(23) Xi, P.; Xu, Z.; Gao, D.; Chen, F.; Xue, D.; Tao, C. L.; Chen, Z. N. Solvothermal Synthesis of Magnetic Copper Nitride Nanocubes with Highly Electrocatalytic Reduction Properties. *RSC Adv.* **2014**, *4*, 14206−14209.
(24) Wiley, B.; Sun, Y.; Xia, Y. Synthesis of Silver Nanostructures with Controlled Shapes and Properties. *Acc. Chem. Res.* **2007**, *40*, 1067−1076.
(25) Li, Q.; Zhu, W.; Fu, J.; Zhang, H.; Wu, G.; Sun, S. Controlled Assembly of Cu Nanoparticles on Pyridinic-N Rich Graphene for Electrochemical Reduction of CO_2 to Ethylene. *Nano Energy* **2016**, *24*, 1−9.
(26) Kortlever, R.; Peters, I.; Koper, S.; Koper, M. T. M. Electrochemical CO_2 Reduction to Formic Acid at Low Overpotential and with High Faradaic Efficiency on Carbon-Supported Bimetallic Pd-Pt Nanoparticles. *ACS Catal.* **2015**, *5*, 3916−3923.
(27) Li, C. W.; Kanan, M. W. CO_2 Reduction at low Overpotential on Cu Electrodes Resulting from the Reduction of Thick Cu_2O Films. *J. Am. Chem. Soc.* **2012**, *134*, 7231−7234.
(28) Jung, H.; Lee, S. Y.; Lee, C. W.; Cho, M. K.; Won, D. H.; Kim, C.; Oh, H. S.; Min, B. K.; Hwang, Y. J. Electrochemical Fragmentation of Cu_2O Nanoparticles Enhancing Selective C-C Coupling from CO_2 Reduction Reaction. *J. Am. Chem. Soc.* **2019**, *141*, 4624−4633.
(29) Grosse, P.; Gao, D.; Scholten, F.; Sinev, I.; Mistry, H.; Roldan Cuenya, B. Dynamic Changes in the Structure, Chemical State and Catalytic Selectivity of Cu Nanocubes during CO_2 Electroreduction: Size and Support Effects. *Angew. Chem., Int. Ed.* **2018**, *57*, 6192−6197.
(30) Roberts, F. S.; Kuhl, K. P.; Nilsson, A. High Selectivity for Ethylene from Carbon Dioxide Reduction over Copper Nanocube Electrocatalysts. *Angew. Chem., Int. Ed.* **2015**, *54*, 5179−5182.
(31) Loiudice, A.; Lobaccaro, P.; Kamali, E. A.; Thao, T.; Huang, B. H.; Ager, J. W.; Buonsanti, R. Tailoring Copper Nanocrystals towards C2 Products in Electrochemical CO_2 Reduction. *Angew. Chem., Int. Ed.* **2016**, *55*, 5789−5792.
(32) Yang, H. J.; He, S. Y.; Chen, H. L.; Tuan, H. Y. Monodisperse Copper Nanocubes: Synthesis, Self-Assembly, and Large-Area Dense-Packed Films. *Chem. Mater.* **2014**, *26*, 1785−1793.
(33) Goodpaster, J. D.; Bell, A. T.; Head-Gordon, M. Identification of Possible Pathways for C-C Bond Formation during Electrochemical Reduction of CO_2: New Theoretical Insights from an Improved Electrochemical Model. *J. Phys. Chem. Lett.* **2016**, *7*, 1471−1477.
(34) Bronsted, J. N. Acid and Basic Catalysis. *Chem. Rev.* **1928**, *5*, 231−338.
(35) Bell, R. P. The Theory of Reactions Involving Proton Transfers. *Proc. R. Soc. London, Ser. A* **1936**, *154*, 414.
(36) Evans, M. G.; Polanyi, M. Inertia and Driving Force of Chemical Reactions. *Trans. Faraday Soc.* **1938**, *34*, 11−23.

DOI: 10.1021/acs.nanolett.9b03324
Nano Lett. 2019, 19, 8658−8663